lubricants

MDPI

Article

Lubrication Performance Promotion of GTL Base Oil by BN Nanosheets via Cascade Centrifugation-Assisted Liquid-Phase Exfoliation

Jiashun Liu [1,†], Shuo Xiang [1,†], Xiaoyu Zhou [2], Shigang Lin [1,*], Kehong Dong [3], Yiwei Liu [1], Donghai He [1,*], Yunhong Fan [4], Yuehao Liu [4], Bingxue Xiong [4], Kai Ma [4], Kaiyang Xiao [1], Genmao Luo [1], Qinhui Zhang [1] and Xin Yang [1]

[1] Army Logistics Academy of PLA, Chongqing 401331, China; xslaplace@163.com (S.X.)
[2] Unit 63936, Beijing 102205, China
[3] Unit 77576, Lhasa 851400, China
[4] Sinopec Lubricant Co., Ltd., Synthetic Lubes Branch, Chongqing 400039, China
* Correspondence: linshigang2024@163.com (S.L.); 15998991983@163.com (D.H.)
† These authors contributed equally to this work.

Abstract

Broad lateral size and thickness distributions impede the application of hexagonal boron nitride nanosheets (BNNSs) as friction modifiers in base oil, although they possess remarkable potential for lubrication performance promotion. In this work, a cascade centrifugation-assisted liquid-phase exfoliation approach was presented to prepare BNNSs from hexagonal boron nitride (h-BN) efficiently and scalably. Subsequently, they were ultrasonically dispersed into gas-to-liquid (GTL) base oil, and their lubrication performance promotion was evaluated by a four-ball tribotester. Tribological tests demonstrated that BNNS possesses excellent friction-reducing and anti-wear properties in GTL. Furthermore, the findings indicate that at a BNNS content of 0.8 wt.%, the system displayed the lowest COF and WSD. Particularly, with an addition of 0.8 wt.% BNNS into GTL, the AFC and WSD are reduced significantly by 40.1% and 35.4% compared to pure base oil, respectively, and the surface roughness, wear depth, and wear volume were effectively reduced by 91.0%, 68.5%, and 76.8% compared to GTL base oil, respectively. Raman, SEM-EDS, and XPS results proved that the outstanding friction-reducing and anti-wear properties of BNNS can mainly be ascribed to the presence of physical adsorption film and tribo-chemical film, which were composed of FeOOH, FeO, Fe_3O_4, and B_2O_3.

Keywords: lubrication performance; hexagonal boron nitride nanosheets; GTL base oil; liquid-phase exfoliation

check for updates

Received: 12 May 2025
Revised: 7 June 2025
Accepted: 20 June 2025
Published: 23 June 2025

Citation: Liu, J.; Xiang, S.; Zhou, X.; Lin, S.; Dong, K.; Liu, Y.; He, D.; Fan, Y.; Liu, Y.; Xiong, B.; et al. Lubrication Performance Promotion of GTL Base Oil by BN Nanosheets via Cascade Centrifugation-Assisted Liquid-Phase Exfoliation. *Lubricants* **2025**, *13*, 281. https://doi.org/10.3390/lubricants13070281

Copyright: © 2025 by the authors. Licensee MDPI, Basel, Switzerland. This article is an open access article distributed under the terms and conditions of the Creative Commons Attribution (CC BY) license (https://creativecommons.org/licenses/by/4.0/).

1. Introduction

In mechanical systems, friction and wear constitute a large proportion of the energy dissipation and failure of physical components [1]. It is estimated that 30–50% of the world's fuel energy is used to overcome the frictional forces resulting from the interaction of surfaces [2,3]. To reduce mechanical energy dissipation and failure [4,5], the use of appropriate lubricants is considered an effective strategy [6,7]. Lubricating oil is made up of 80–90% base oil and 10–20% additives. As known as "chips" of lubricating oils, additives could considerably enhance the performance of lubricants and extend the equipment life, resulting from the improvement in the wear resistance, friction-reducing, and thermal

stability performance of base oils [8]. However, conventional additives cannot meet the growing demands of lubricating oils in terms of toxicity and biodegradability [9], as they are harmful to human bodies and toxic to the environment because they incorporate heavy metals, halogens, and sulfur compounds [10].

From this perspective, it is of particular importance to select a suitable new type of additive. Nanoparticles, the sizes of which in all three dimensions are not more than 100 nm, could play a key role in lubrication, since they can easily enter the friction contact region, preventing the rubbed metal surfaces from coming into direct contact [11,12]. In comparison with conventional additives, nano-additives can withstand severe operating conditions, such as high loads and speeds [13], additionally improving the tribological performance of mechanical components [14]. As lubricant additives, nanoparticles, including metallic nanoparticles (e.g., Cu, Ag, Ni) [15], metal oxides (e.g., ZnO, TiO_2, Al_2O_3 [7], metal sulfides (e.g., MoS_2, WS_2) [16], carbon-based materials (e.g., Graphene, CNTs, Diamond NPs) [17], and other nanocomposites [18], demonstrate exceptional tribological properties, such as reduced friction and increased wear resistance. Numerous experimental results have demonstrated the close relationship between the size of nano-additives and their tribological properties [7,19]. Shen [20] demonstrated that the maximum wear depth increases with an increasing size of nanomaterials, while the friction coefficient (COF) demonstrates the most complex changes at medium particle sizes. Alves [8] has investigated the effects of the size and addition of CuO nanoparticles (NPs) on nano-lubrication mechanisms and has found that the COF increases as the particle size decreases. Sun [21] investigated the effect of five different SiO_2 particle-size scales on friction mechanisms. These results indicate that the transformation of friction mechanisms is significantly influenced by particle size. Xu [14] discovered that using uniform-sized particles can decrease the wear rate by 7–9% when compared to systems with varying particle sizes. Additionally, a lubrication system that incorporates both large and small Cu nanoparticles can achieve a maximum reduction of 67.88% in the average friction force compared to a system that only uses uniformly large particles. Such results indicate that the use of Cu NPs with small, uniform particle sizes results in superior tribological properties compared to those with dispersed particle sizes. Han [8] observed that the first-rank wear resistance and load-carrying capacity occurred at a specific Cu-Fe nanoparticle (NP) size ratio. Kumar [10] investigated how graphite particles of four different sizes—50 nm, 450 nm, 4 microns, and 10 microns—when added in equal amounts to grease, affected its anti-friction, anti-wear, and extreme-pressure properties. He concluded that smaller graphite particles lead to improved tribological performance. Dong [22] conducted a comprehensive study on the influence of black phosphorus nanosheet size on the COF and wear rate of a Ti_6Al_4V alloy as a water-based lubrication additive. The study found that the COFs and wear rates of different black phosphorus nanosheet sizes decreased to varying degrees, with small-sized black phosphorus quantum dots exhibiting excellent wear resistance and significantly reducing the COF and wear rate.

BNNS, as a promising additive, exhibits extensive potential for development in various fields due to its unique physical properties and superior friction performance. In recent years, considerable research efforts have been devoted to enhancing the lubricating performance of BNNS with multiple routes. For example, Shan [23] has investigated the esterified cellulose-assisted in situ exfoliation (ECAIE) technique for producing h-BNNS as a two-dimensional material. This process has achieved a lateral size of h-BNNS of up to 1200 nm, leading to a noteworthy decrease in the friction coefficient by 340% and a reduction in the wear rate by 220% on steel surfaces. Kumari [24] has implemented an innovative method for creating h-BNNS through strong alkali-assisted hydrothermal exfoliation and defect-sensitive etching. The h-BNNS incorporated into SN-150 mineral

lubricant base oil enhanced the oil's lubrication characteristics by reducing friction by 34% and wear volume by 75%. Wang [25] introduced a method for producing BNNS using alkylamine-assisted ball milling, which is simple and cost-effective. This approach provides a new pathway for creating lipophilic BNNS for use in lubrication and friction applications. In the study, the lipophilic BNNS-TOA that was prepared could decrease the friction coefficient by 20.2%. Additionally, the width of the wear scar had been diminished by 75%, and the depth of the wear scar had notably become shallower. The studies mentioned have demonstrated that BNNSs synthesized in various ways can serve as effective lubrication additives, exhibiting strong anti-friction and anti-wear properties. However, the lubricating mechanisms of BNNS vary, suggesting that certain morphologies of BNNS may provide optimum anti-friction and anti-wear performance.

In this study, BNNS was produced via the sonication-assisted liquid-phase exfoliation method. The obtained BNNS was characterized through multiple techniques, involving powder X-ray diffraction (XRD), Fourier-transform infrared (FT-IR) spectroscopy, and Raman spectra (Raman). In order to determine the concentration of BNNS that has the most significant influence on anti-wear and friction-reducing properties, the tribological properties of as-synthesized BNNS samples in GTL base oil were investigated using a four-ball tribotester. Raman spectroscopy and a 3D optical profiler were used to analyze the wear surface. The composition and microstructure of the tribo-chemical film were analyzed using a scanning electron microscope (SEM), energy-dispersive spectroscopy (EDS), and X-ray photoelectron spectroscopy (XPS). These analyses revealed that the lubrication performance of GTL base oil can be promoted by BNNS remarkably. The lubrication mechanism of BNNS in GTL base oil was discussed further.

2. Experimental Details

2.1. Materials

h-BN was supplied by the Su Zhou Hengqiu Graphene Technology Co., LTD. (Suzhou, China). GTL base oil (the typical characteristics are shown in Table 1) was commercially procured from the Shell Hong Kong Co., LTD (Hong Kong, China). Bearing steel balls composed of GCr15 bearing steel with a diameter of 12.7 mm and a hardness of HRC 60–65 were obtained from the SINOPEC Research Institute of Petroleum Processing Co., Ltd. (Beijing, China). Absolute ethyl alcohol, isopropanol, and petroleum ether were received from Chengdu Kelong Chemical Reagent Co., Ltd. (Chengdu, China).

Table 1. The typical physicochemical properties of GTL base oil.

Test Description	Result	Method
Kinematic viscosity (mm^2/s) (40 °C)	44.23	ASTM D445
Kinematic viscosity (mm^2/s) (100 °C)	7.615	ASTM D445
Viscosity Index	140	ASTM D2270
Appearance	Clear to bright	Visual
Color (ASTM) (Quantitative)	0.5	ASTM D1500
Color (Seibert color)	30	ASTM D156
Density (kg/m^3) (15 °C)	827.7	ASTM D4052
Refractive index (20 °C)	1.46	ASTM D1218
Pour point (°C)	−45	ASTM D6749
Flash point (°C) (PMcc)	234	ASTM D93

2.2. Preparation of GTL Base Oil with BNNS

BNNSs were synthesized via cascade centrifugation-assisted liquid-phase exfoliation, as illustrated in Figure 1. A total of 5 g of h-BN powder was dispersed in a 500 mL mixture of isopropanol and deionized water (2:1 v/v IPA: DIW). Subsequently, the mixed solution

was sonicated for 12 h using a sonicator (ultrasonic instrument, Kunshan, China) at a power of 480 W, with the sonication set to operate for 30 s and then pause for 10 s in each cycle. After standing for 12 h, the mixed solution was centrifuged at 1 krpm for 3 min (H2500R centrifuge, Changsha, China), and the supernatants were extracted from the precipitate at the bottom, which were labeled as the "1 krpm" samples. The "1 krpm" samples were then poured into to a new tube to be centrifuged at 2 krpm for 3 min, and the supernatants were subsequently extracted, which were labeled as the "2 krpm" samples. The procedure was carried out repeatedly at 3, 4, 5, 6, and 7 krpm. The "7 krpm" samples were then added into a new tube to be centrifuged at 8 krpm for 3 min, and the precipitate was collected and the residual solvents were removed by the freeze-drying method. The obtained powders were h-BN nanosheets (abbreviated as BNNSs) [26].

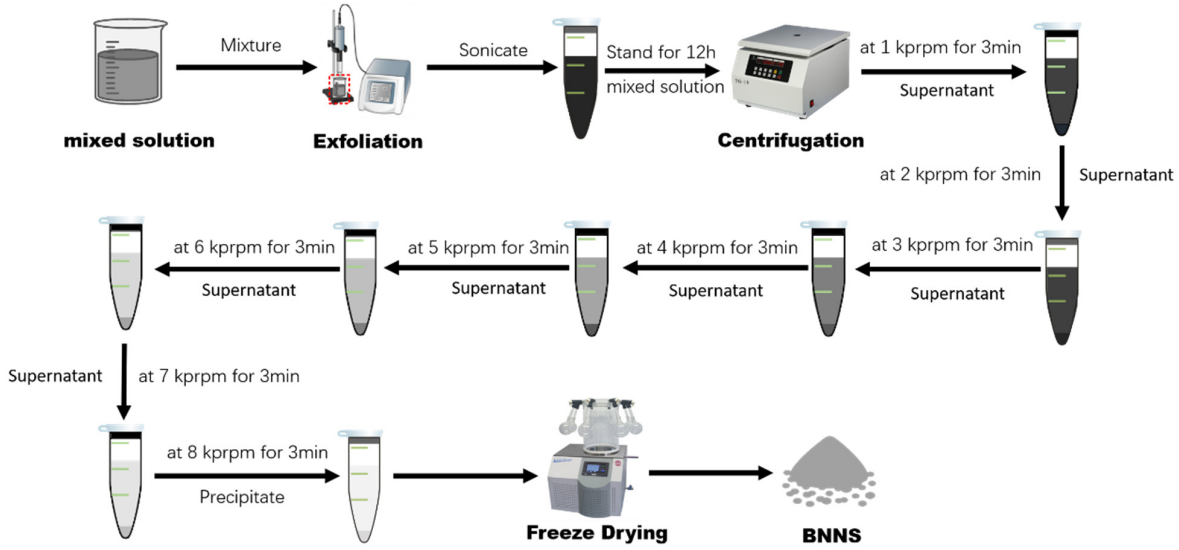

Figure 1. Preparation of BNNS via cascade centrifugation-assisted liquid-phase exfoliation.

The crystal structure of h-BN and BNNS was analyzed by powder X-ray diffraction (XRD, Bruker D8 ADVANCE, XRD, Bruker D8 ADVANCE, Berlin, Germany) with Cu Kα radiation in the 2θ range from 5° to 90° for 21 min. The Raman spectra of h-BN and BNNS were obtained using a Renishaw Invia spectrometer with an excitation wavelength of 532 nm. The morphologies of BNNS samples were observed by field-emission scanning electron microscopy (SEM, Quanta250 EFG, FEI, Waltham, MA, USA), transmission electron microscopy (TEM), and high-resolution transmission electron microscopy (HRTEM, FEI Tecnai F30, acceleration voltage: 300 kV). The thickness of BNNS was determined by atomic force microscopy (AFM, Bruker, Camarillo, CA, USA) under ambient conditions. AFM images were obtained under tapping mode with a scan resolution of 512 × 512 pixels and a scan rate of 0.1 Hz. Infrared spectroscopy of h-BN and BNNS was performed on a Fourier-transform infrared spectrometer (FT-IR PerkinElmer Spectrum, Waltham, MA, USA) at a resolution of 4 cm^{-1}.

2.3. Tribology Tests and Analysis

A four-ball tribometer was employed to explore the anti-wear and friction-reducing properties of GTL base oil with various concentrations of BNNS, as shown in Figure 2. The tribometer configuration consists of four balls arranged in an equilateral tetrahedron, where the upper rotating ball contacts the three stationary lower balls as exhibited in Figure 2b,c, respectively. Friction experiments were conducted under loads ranging from 100 to 600 N, at a rotation speed of 1200 rpm and room temperature (25 ± 2 °C) for 60 min according to the standard of NB/SH/T 0189-2017. The maximum contact pressure and lambda ratio

were calculated using the Hertzian point contact theory and the Dowson and Hamrock minimum film thickness formula, respectively. Based on these calculations, the contact area achieved a boundary lubrication regime in this study. GTL was used as the base oil, and the friction couple was completely immersed in 100 mL of lubricating oil. Prior to the tribotest, the friction couple was rinsed in a 200 W ultrasonic bath to remove rust grease from the surface with petroleum ether for 25 min followed by air-drying in a ventilated place.

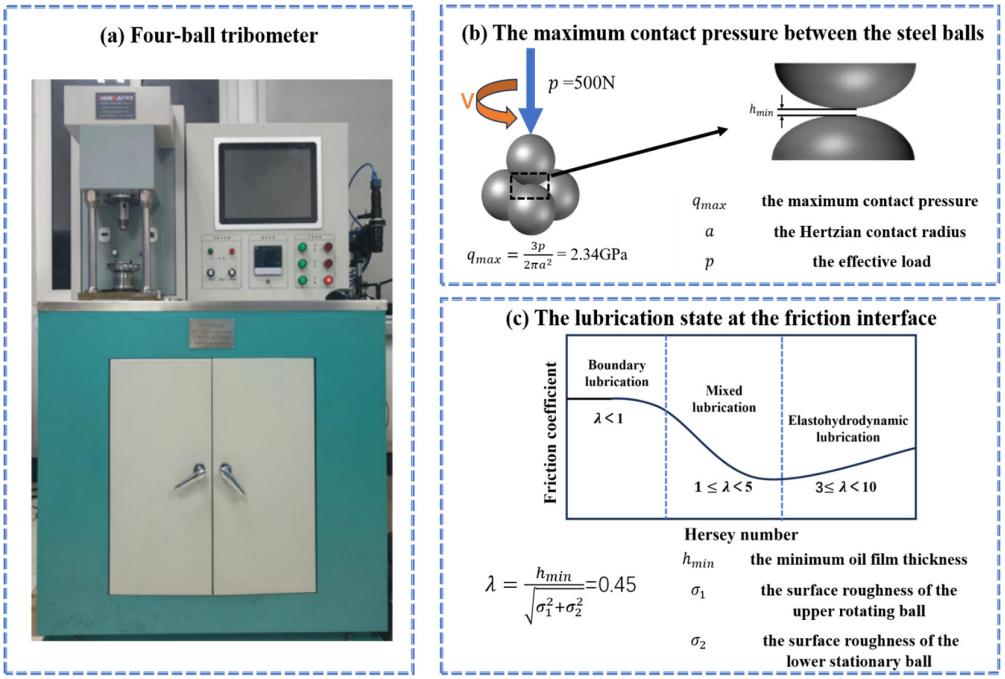

Figure 2. The four-ball tribometer schematic diagram. (**a**) Real image of tribometer, (**b**) 3D view, and (**c**) force analysis between balls.

Following the tribotest, the coefficient of friction (COF) was automatically recorded via the computer system, while the wear scar diameter (WSD) on the three fixed balls was measured using an optical microscope. The surface roughness, wear depth, and wear volume were obtained using the 3D optical profiler. To guarantee the repeatability and accuracy of the data, every test was replicated three times and the average value was calculated. The parameters of the tested steel balls are detailed in Table 2.

Table 2. Experimental parameters and basic characteristics of the steel balls used.

Parameter	GTL Base Oil	0.2 wt.% BNNS	0.4 wt.% BNNS	0.6 wt.% BNNS	0.8 wt.% BNNS	1.0 wt.% BNNS	10.0 wt.% BNNS
Speed	1200 r/min						
Load	500 N						
Temperature	40 °C						
Test Duration	60 min						
Component	**Elastic modulus**	**Poisson ratio**	**Diameter**		**Rockwell**	**Surface roughness**	
GCr15	2.085×10^5 Mpa	0.3	12.7 mm		60 ± 1	0.256 μm	

After the tribotests, the steel balls were collected and ultrasonically washed with acetone. The morphology of the worn surface was then examined using an S-3700N electron microscope (Hitachi, Tokyo, Japan) and 3D optical profilers (Nanovea, Irwindale, Irvine,

CA, USA). The elemental distribution and composition over the worn surface were analyzed and quantified using an Oxford X-Max 20 mm^2 energy-dispersive X-ray spectrometer (Oxford Instruments, Oxford, UK). Raman spectrometry (LabRAM HR Evolution, HORIBA, Longjumeau, France) with a laser wavelength of 1365 nm was used to determine the Raman spectra of worn surfaces. To further measure the elemental composition and chemical state of the ternary films on the worn surfaces, X-ray photoelectron spectroscopy replication (XPS) tests were conducted using an ESCALAB MKII X-ray photoelectron spectrometer (Thermo-VG Scientific, Waltham, MA, USA) to probe the deposition of the tribo-films.

3. Results and Discussion

3.1. Characterization of BNNS

The morphological characteristics of pristine h-BN and the exfoliated BNNS are presented in Figure 3. Figure 3a,b show the SEM images of pristine h-BN and BNNS, respectively. Pristine h-BN exhibits an opaque, laminated structure with lateral dimensions of approximately 0.5~5 μm and initial thicknesses exceeding 100 nm. In contrast, BNNS exhibits thinner and smaller products with particle sizes ranging from 100 to 500 nm after the effective exfoliation process. The atomic force microscopy (AFM) image (Figure 3c) reveals that the majority of the exfoliated BNNS is around 50 nm. The morphology of these BNNSs was further elucidated by TEM (Figure 3d) and HRTEM (Figure 3e,f) [27]. As evident from Figure 3d, multiple ultrathin BNNSs cover the supporting film, exhibiting morphological characteristics consistent with the SEM image. The high-resolution TEM image (Figure 3f, left), in conjunction with the selected area electron diffraction (SAED) (Figure 3f, upper right) and inverse fast Fourier transform (IFFT) (Figure 3f, lower right), confirms the hexagonal atomic configuration of BNNS. The inset in the SAED pattern demonstrates that the BNNS maintains its well-crystallized structure throughout the exfoliation process. Furthermore, the inset in the IFFT image shows that the center distance between adjacent hexagonal rings is 0.25 nm, corresponding to the (002) plane [28].

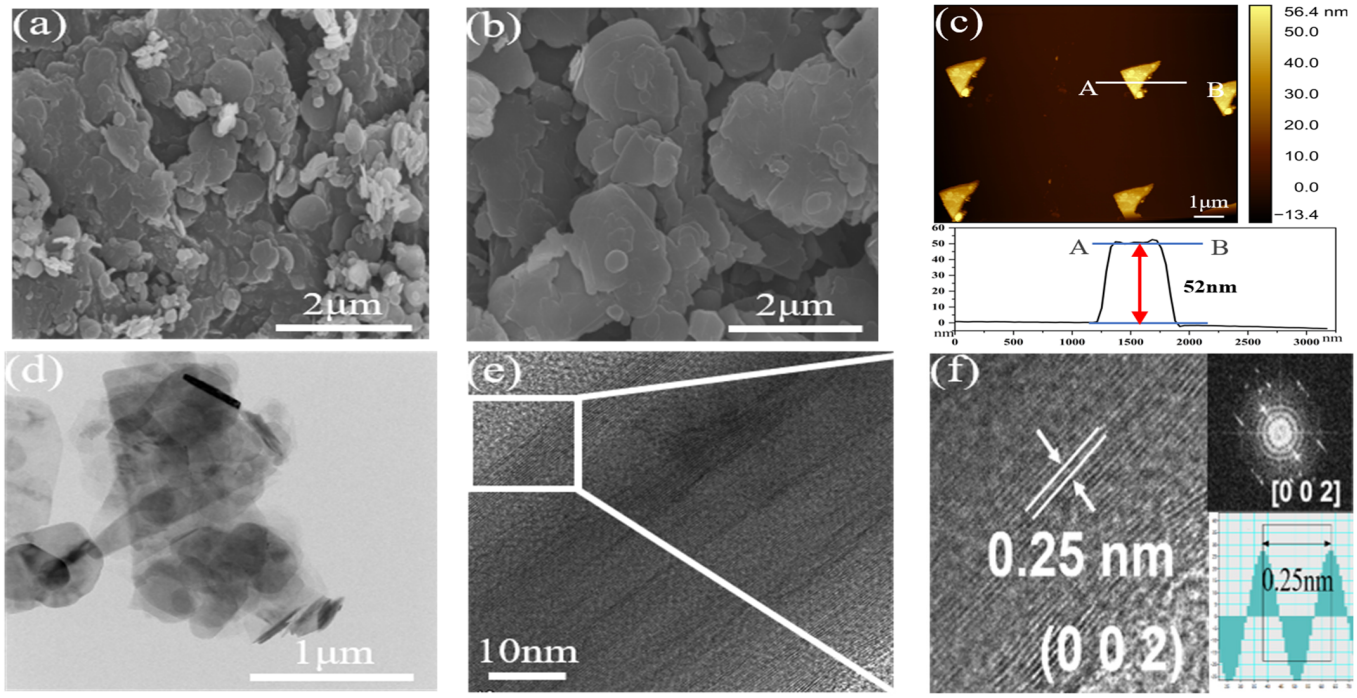

Figure 3. SEM images of pristine h-BN (**a**) and BNNS (**b**), AFM image (**c**), TEM images of BNNS (**d**,**e**), and high-resolution TEM image of BNNS (left) and its IFFT image (right) (**f**).

XRD patterns of the pristine h-BN and BNNS are compared in Figure 4a. The obtained XRD patterns of h-BN exhibit characteristic peaks at 2θ~26.58°, 41.51°, 43.73°, 50.11°, and 54.95°, ascribed to the (002), (100), (101), (102), and (004) planes, respectively. On the contrary, the BNNS diffraction peaks demonstrate a reduced intensity and sharpness, consistent with their weakened c-direction stacking [29]. BNNS has a dominant peak at 2θ = 26.56°, showing a slight but discernible low-angle shift compared to pristine h-BN (26.58°), with this shift resulting from reduced crystallinity due to the exfoliation process [30]. Both the full width at half maximum (FWHM) and cos θ of BNNS have shown significant increases compared to h-BN, indicating that the thickness of BNNS decreases [31]. The diffraction peaks of BNNS maintain consistency with those of h-BN, implying that the liquid-phase exfoliation process preserves the structural integrity of BNNS without introducing detectable impurities. Figure 4b shows the FTIR spectra of pristine h-BN and BNNS. The h-BN has two characteristic peaks at 1370 and 805 cm^{-1}, presenting the stretching vibration of sp2-bonded B–N and the bending vibration of B–N–B, respectively [32]. When the h-BN was exfoliated into BNNS, the two characteristic peaks shifted to 1376 and 817 cm^{-1}, resulting from the stretching vibration and, specifically, bending vibration of B–N bonds. As presented in Figure 4c, the strong peak at 1364 cm^{-1} presents the high-frequency interlayer Raman-active E_{2g} mode of pristine h-BN. The strong peak shifts to 1365 cm^{-1} with an increased full width at half maximum, indicating the reduced interlayer interaction of BNNS [32], which accords with the XRD and FTIR results.

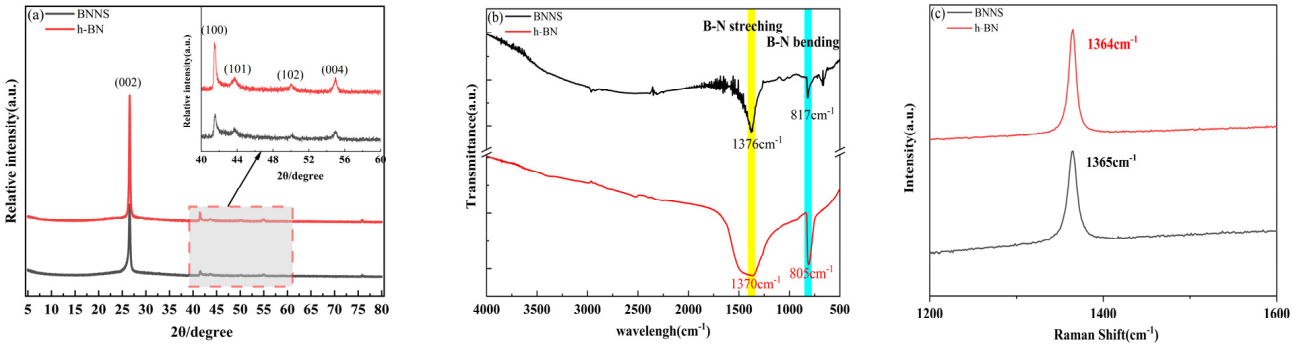

Figure 4. (**a**) XRD pattern, (**b**) FTIR spectra, and (**c**) Raman spectra of the pristine h-BN and BNNS.

3.2. Friction and Wear Performance

The nanomaterial additives had beneficial effects on the friction-reducing and anti-wear properties of the lubricating oil and indicated that there exists an optimal addition of nanomaterial additives. Therefore, a series of different concentrations was prepared to acquire the optimal additive addition that would result in optimum lubrication performance promotion. Figure 5 presents the evolution of the COF, AFC, and WSD for GTL base oil containing 0 wt.%, 0.1 wt.%, 0.2 wt.%, 0.3wt.%, 0.4 wt.%, 0.6 wt.%, 0.8 wt.%, 1.0 wt.%, and 10.0 wt.% BNNS during the friction test.

As can be seen in Figure 5a, the COF of GTL base oil fluctuates up and down in the initial 70s and then decreases rapidly, resulting from the increase in the actual contact area, which leads to a decrease in the contact pressure after the initial 70s of severe wear. Conversely, the COF of GTL base oil with 0.8 wt.% BNNS decreases dramatically in the initial 50s, then stabilizes, and fluctuates relatively after 50s. Compared with GTL base oil, the COF of GTL base oil with 0.8 wt.% BNNS is smoother and lower, which may be ascribed to the excellent anti-friction properties of the BNNS. Figure 5b visually displays the AFC and WSD values of GTL base oil with various concentrations of BNNS, where the AFC and WSD are reduced significantly by 40.1% and 35.4%, respectively, for the GTL base

oil in contrast with the GTL base oil with 0.8 wt.% BNNS, which could be explained by the outstanding anti-wear properties of the BNNS [33].

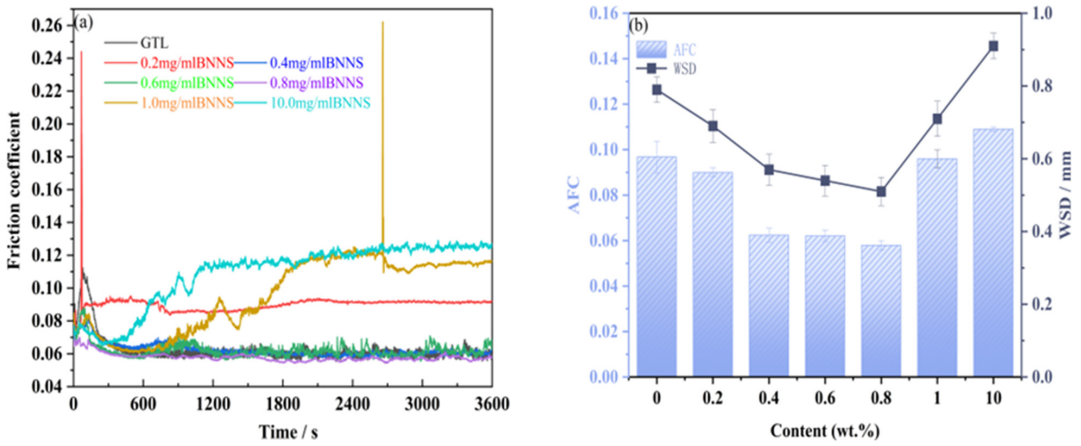

Figure 5. The COF (**a**), AFC, and WSD (**b**) of GTL base oil with different concentrations of BNNS (60 min, 40 °C, 1200 rpm, 500 N).

In order to investigate the wear resistance of GTL base oil and GTL base oil with BNNS, the surface roughness, wear depth, and wear volume were observed using a 3D optical profiler, as demonstrated in Figure 6.

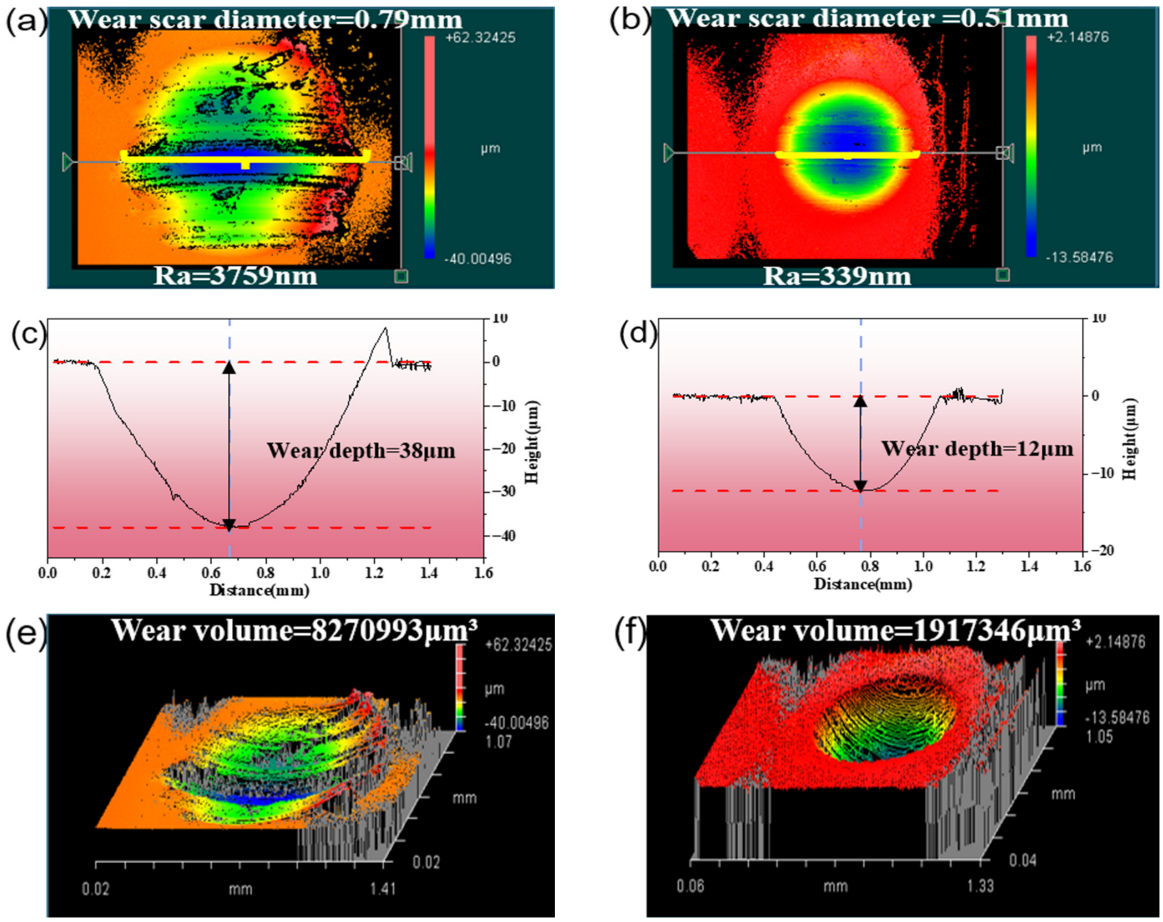

Figure 6. 2D wear surface topographies, cross-sectional profile, and 3D wear surface topographies of steel balls lubricated with GTL base oil (**a**,**c**,**e**) and GTL base oil with 0.8 wt.% BNNS (**b**,**d**,**f**) (60 min, 40 °C, 1200 rpm, 500 N).

As shown in Figure 6a,b, the wear surface of the steel balls lubricated by GTL base oil appears to have a higher surface roughness of roughly 3759 nm. Furthermore, more severe worn scratches were discerned in comparison with those on steel balls lubricated by GTL base oil with 0.8 wt.% BNNS. After the introduction of 0.8 wt.% BNNS into the base oil, the surface roughness, wear depth, and wear volume were effectively reduced by 91.0%, 68.5%, and 76.8%, respectively. This is due to the adsorption of BNNS on the steel balls, which alters the characteristics of the surface and protects the two contact surfaces from severe wear as much as possible [34].

3.3. Worn Surface Analysis

To detect the formation of tribo-film during lubrication using GTL base oil with 0.8 wt.% BNNS, the Raman spectra of the wear surfaces were further collected after the tribotest (Figure 7). Compared with the Raman spectra of the wear surface lubricated by the GTL base oil, the characteristic peak at about 1365 cm^{-1} appears on the wear surface lubricated by the GTL base oil with 0.8 wt.% BNNS, which is similar to in the Raman spectra of the BNNS itself. The results demonstrate that BNNS in GTL base oil can readily enter into the interface to avoid direct contact and relieve damage to steel balls [35].

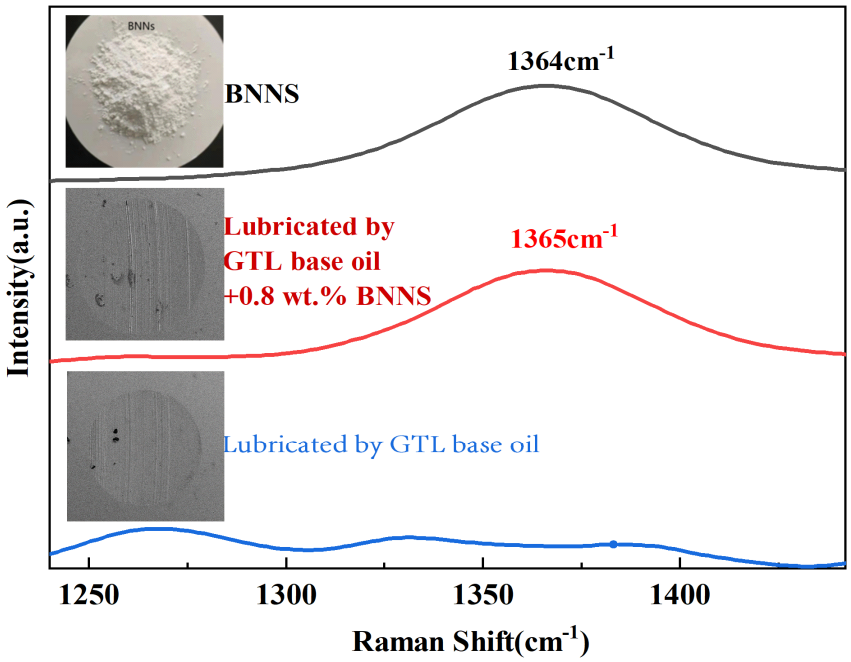

Figure 7. Raman spectra of BNNS, the wear surface of the steel ball lubricated by GTL base oil, and that of the steel ball lubricated by GTL base oil with 0.8 wt.% BNNS.

The morphology of the wear surface of the steel ball lubricated by GTL base oil and GTL base oil with 0.8 wt.% BNNS was observed by SEM, and the corresponding element distribution at the wear scar position was determined by the equipped EDS, as demonstrated in Figures 8 and 9, respectively. When pure GTL base oil was used as the lubricant, the steel ball surface displayed severe wear with numerous deep furrows (Figure 8). Conversely, the wear surface of the steel ball lubricated by the GTL base oil with 0.8 wt.% BNNS was smoother with little visible wear (Figure 9). These results demonstrate that BNNS can obviously relieve the wear of the steel ball friction pair. Furthermore, according to the EDS mapping results of the steel ball surface, the contact area contains various concentrations of C, O, Fe, B, and N elements (Figure 9), while no detectable B and N elements are discovered in the wear surface corresponding to GTL base oil (Figure 8), implying that BNNSs are easily adsorbed on the steel ball surface. The BNNS that entered

into the two contact surfaces efficiently avoids the direct contact of some of the contact surface's rough peaks, implying that the BNNSs possess extraordinary friction-reducing and anti-wear properties [36].

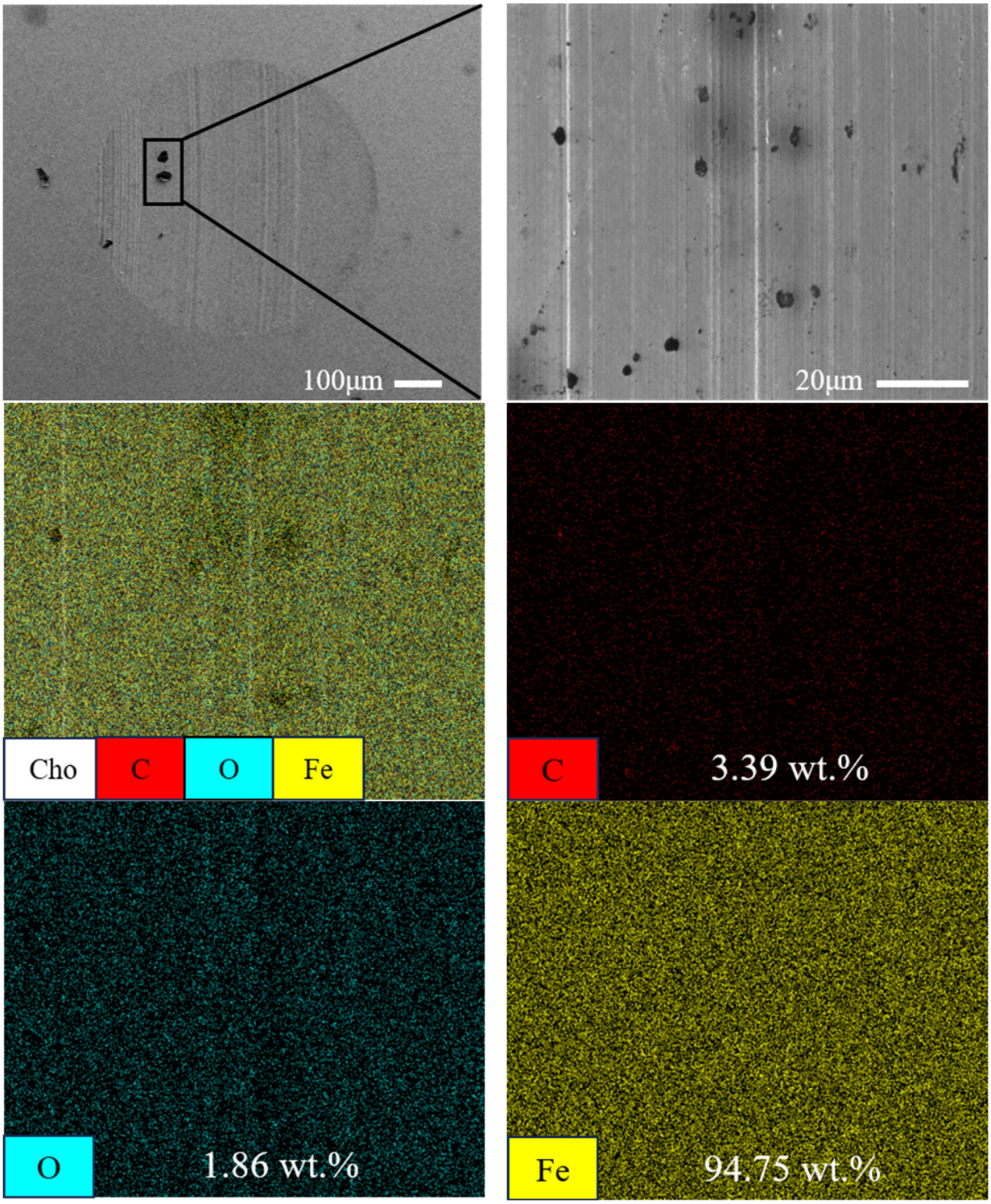

Figure 8. SEM images and EDS element mapping of wear surface of steel ball lubricated by GTL base oil (60 min, 40 °C, 1200 rpm, 500 N).

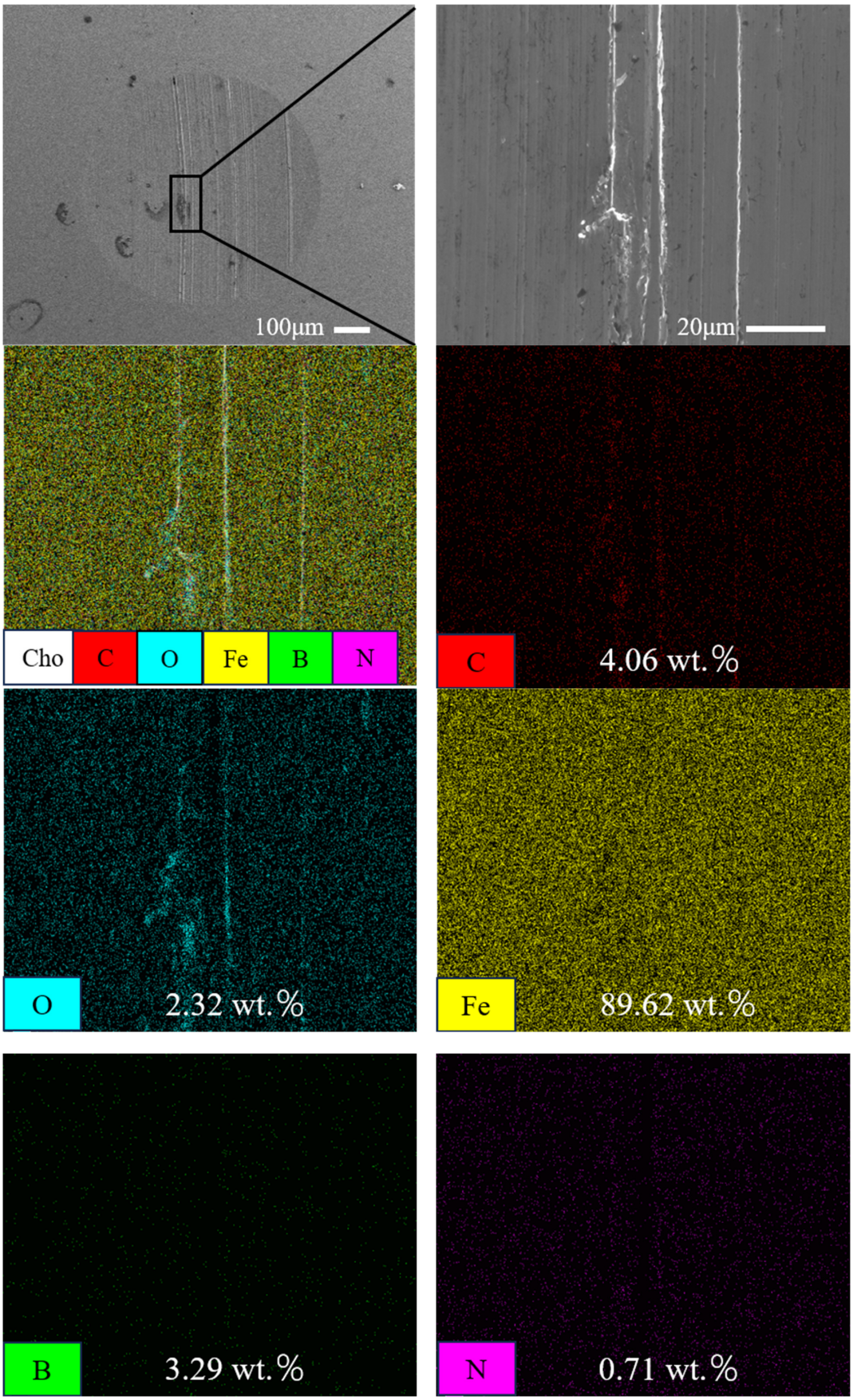

Figure 9. SEM images and EDS element mapping of wear surface of steel ball lubricated by GTL base oil with 0.8 wt.% BNNS (60 min, 40 °C, 1200 rpm, 500 N).

To further elucidate the lubrication mechanism of the BNNS, the chemical bonding state of the wear surface of the steel ball was characterized by XPS, as demonstrated in Figures 10 and 11. The fine spectra of C, O, Fe, B, and N elements are charge-corrected using C 1s of 284.80 eV before fitting. Figure 10 presents the XPS survey of the wear scar lubricated with GTL base oil, showing characteristic peaks for O 1s, C 1s, and Fe 2p. The C 1s spectrum could be deconvoluted into three peaks located at 284.80 eV, 286.63 eV, and 288.68 eV, which can be attributed to C–C or C–H bonds, C–O bonds, and C=O bonds, respectively [37]. All of these likely originate from the partial oxidation and cracking of the GTL base oil during the friction test process (Figure 10b). The peaks of O 1s positioned at approximately 530.08 eV and 531.43 eV are ascribed to metal oxides and the oxidation of hydrocarbon in GTL base oil, respectively. The peaks situated at around 711.08 eV and 724.48 eV are contributed by the Fe 2p1/2 and Fe 2p3/2 of–Fe(III)–O– of Fe_2O_3 [28], respectively, owing to the tribological oxidation production of the steel ball. To further investigate the enhancement of lubrication performance by introducing BNNS as a friction modifier for GTL base oil, we conducted detailed analysis (Figure 11). As shown in Figure 11a, the peaks of C 1s, O 1s, Fe 2p, B 1s, and N 1s are near 284.80 eV, 531.08 eV, 711.08 eV, 188.08 eV, and 400.08 eV, indicating that the BNNS plays a role in the frictional test. The C 1s spectra (Figure 11b) are fitted into three subpeaks at 284.80 eV, 286.48 eV, and 288.83 eV, which belong to C-C or C-H, C–O, and C=O, respectively [37]. The dominant O 1s peak at 531.83 eV and the minor one at 530.28 eV demonstrate the presence of metal oxides and nonmetal oxides on the wear surfaces, respectively. In Figure 11d, the Fe 2p peak at 724.63eV can be ascribed to Fe_3O_4, whereas the Fe 2p peaks at 707.63 eV, 711.33 eV, and 713.48 eV are contributed by FeO, Fe_3O_4, and FeOOH [28]. As shown in Figure 11e, the B 1s peak at 190.19 eV is ascribed to B–N of BNNS, and the B 1s peak at 199.18 eV confirms the formation of the B_2O_3 compound on the wear scar surface, implying that BNNS substantially converts to B_2O_3 during the friction test by a tribo-chemical reaction, which is the same conclusion as in previous research [34]. Moreover, the N 1s peak around 400.03 eV corresponds to organic nitrogen, while the N 1s peak at 398.68 eV corresponds to BNNS, indicating the adsorption of BNNS on the wear surface of the steel balls [28], which is in agreement with the results of the Raman spectra. In conclusion, it is the synergistic combination of physical absorption film and tribo-chemical reaction film that enhances the mechanical strength of the protective film and further promotes the friction-reducing and anti-wear performance.

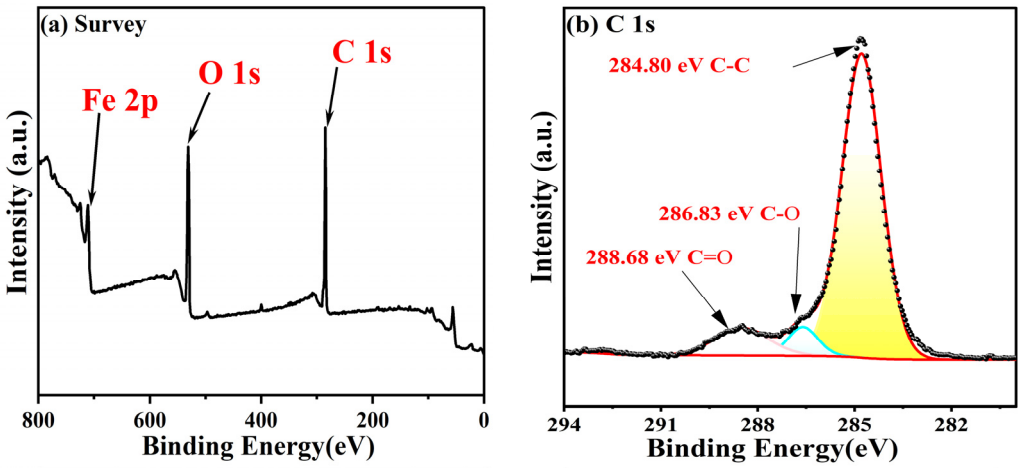

Figure 10. *Cont.*

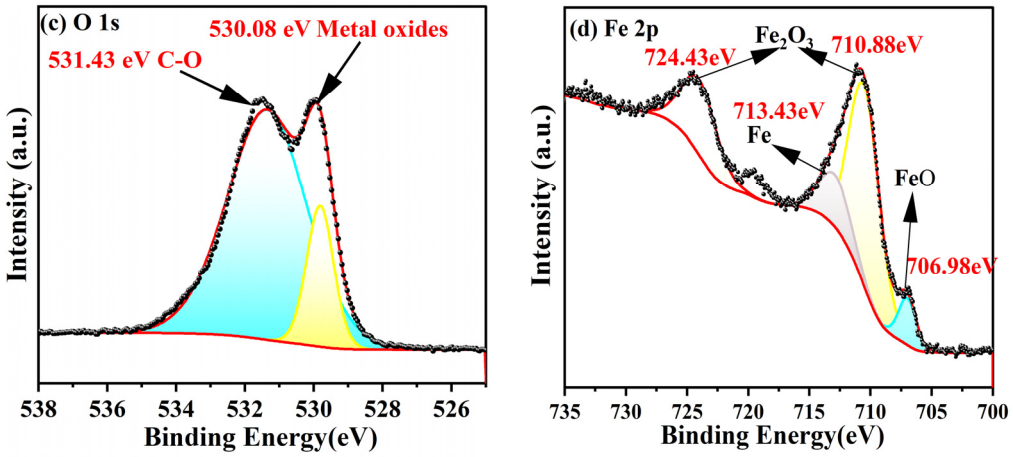

Figure 10. XPS spectra of steel ball wear surface lubricated by GTL base oil. (**a**) XPS survey spectra; (**b**) C 1s fine spectrum; (**c**) O 1s fine spectrum; (**d**) Fe 2p fine spectrum (60 min, 40 °C, 1200 rpm, 500 N).

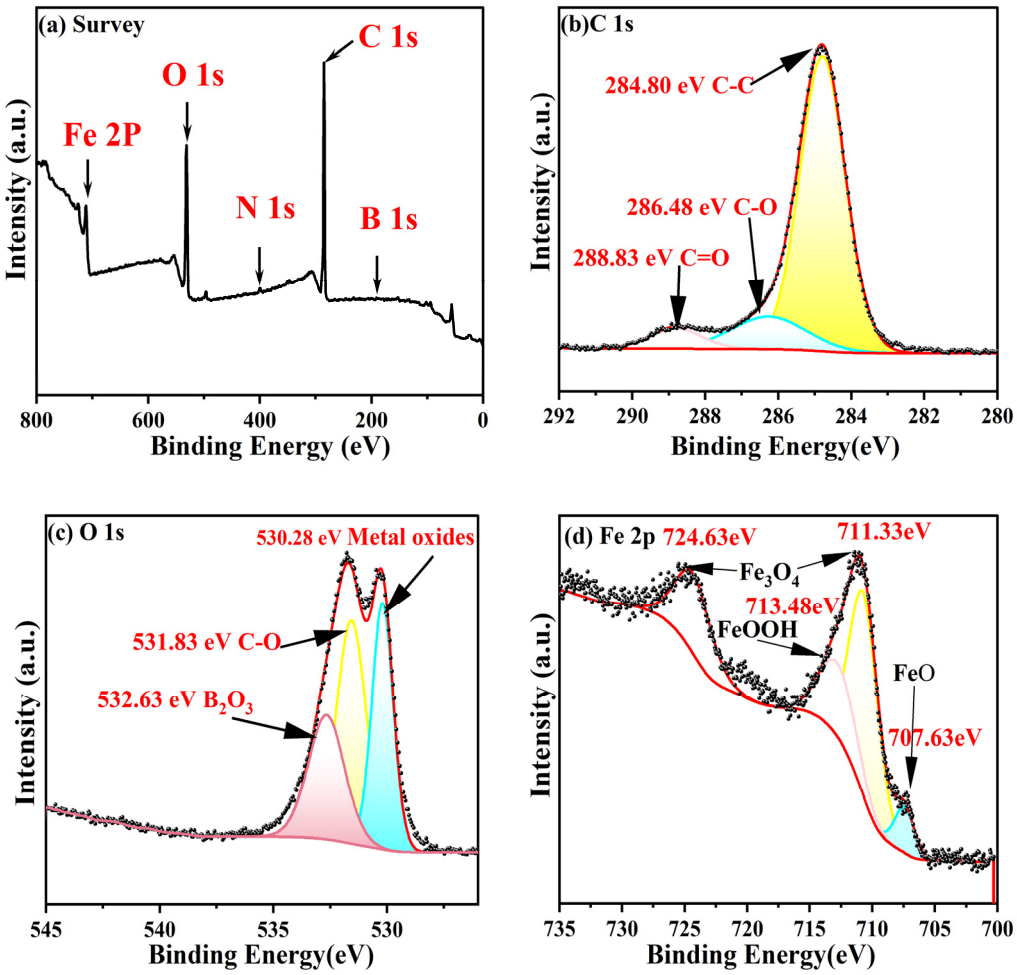

Figure 11. *Cont.*

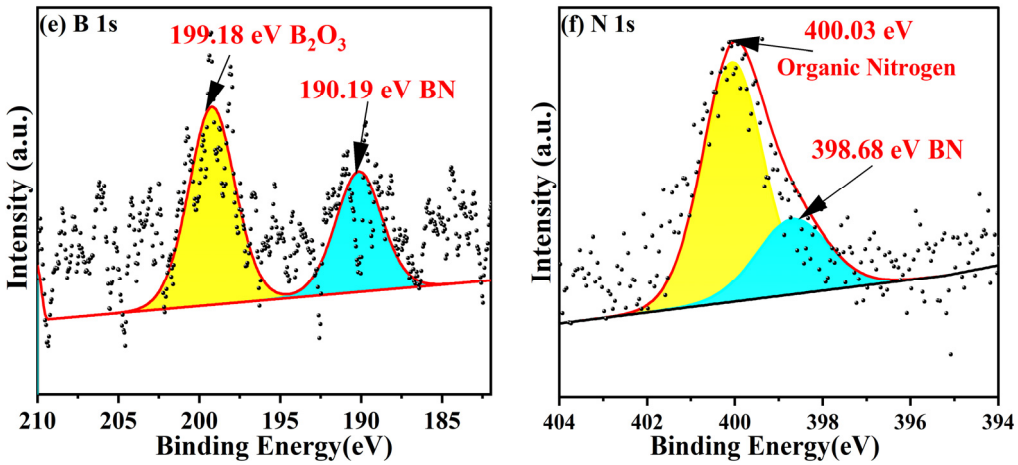

Figure 11. XPS spectra of steel ball wear surface lubricated by GTL base oil with 0.8 wt.% BNNS. (**a**) XPS survey spectra; (**b**) C 1s fine spectrum; (**c**) O 1S fine spectrum; (**d**) Fe 2p fine spectrum; (**e**) B 1s fine spectrum; (**f**) N 1s fine spectrum (60 min, 40 °C, 1200 rpm, 500 N).

3.4. Lubrication Mechanism

Based on the comprehensive tribological analysis, Figure 12 summarizes the proposed lubrication mechanism. After BNNS was introduced into the GTL, the lubricating oil showed outstanding lubrication performance such as a lower AFC, COF, and WSD, as well as smaller wear depth, wear volume, and Ra. The excellent friction-reducing and anti-wear performance originates from the following aspects: During the running-in wear process, the BNNS dispersed in the GTL base oil can readily go into the sliding friction pairs to form a physical adsorption film due to its nano-size effect, which is confirmed by Raman analysis. Furthermore, the 2D layered structure of BNNS allows for effective lubrication by enabling sliding between adjacent layers, which obviously lowers friction and wear [38]. During the steady wear process, the friction coefficient decreases as BNNS and tribochemically derived films form under elevated temperatures and sliding speeds, which prevents the direct contact of the friction pair and reduces the wear volume. Meanwhile, as BNNS breaks and releases free bonds (B-N) under high pressure, the tribo-chemical reaction arises between the lubricant system and the steel contacts, providing an effective tribo-chemical protective film composed of FeOOH, FeO, Fe_3O_4, and B_2O_3, confirmed by XPS analysis. Therefore, it is the superposition of the physical adsorption film and the tribo-chemical reaction film that greatly enhances the strength of the protective film and further contributes to promoting the lubrication performance [39].

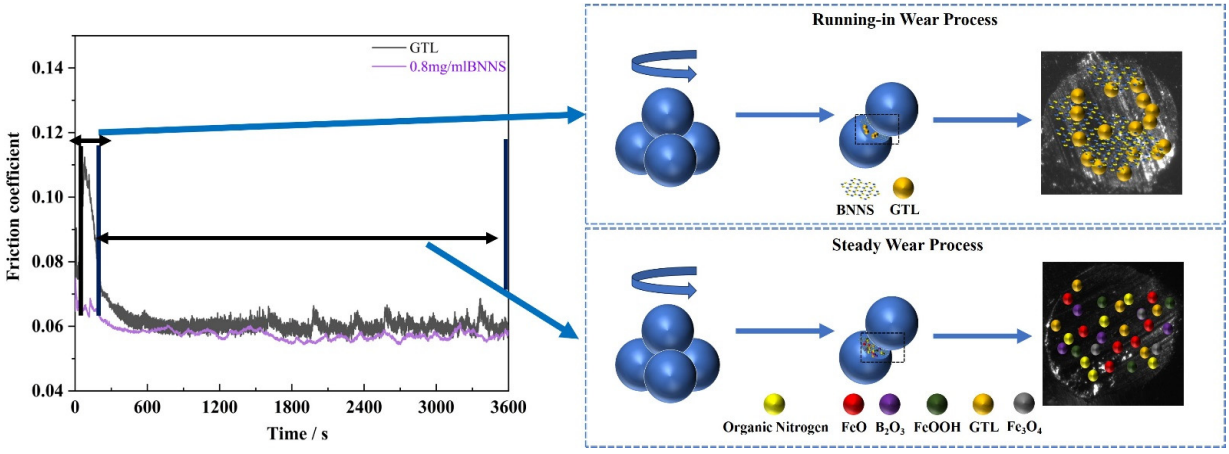

Figure 12. Schematic diagram of the lubricating mechanisms of GTL with BNNS.

4. Conclusions

In this work, a cascade centrifugation-assisted liquid-phase exfoliation approach was presented to prepare hexagonal boron nitride nanosheets (BNNSs) with narrow lateral sizes and thickness distributions from hexagonal boron nitride (h-BN), and the as-prepared BNNSs were characterized through powder X-ray diffraction (XRD), Fourier-transform infrared (FT-IR) spectroscopy, and Raman spectra (Raman). Subsequently, they were ultrasonically dispersed into GTL base oil and their lubrication performance enhancement was evaluated by a four-ball tribotester, while the wear surface of the steel balls was analyzed by Raman spectroscopy, a 3D optical profiler, a scanning electron microscope (SEM), energy-dispersive spectroscopy (EDS), and X-ray photoelectron spectroscopy (XPS). Based on the experimental results and analysis, the principal conclusions can be summarized as follows:

a. The characterization results of BNNS show that it has a lamellar structure with lateral dimensions ranging from 100 to 500 nm and thicknesses around 50 nm. Cascade centrifugation-assisted liquid-phase exfoliation demonstrates high efficiency, rapid processing, and excellent scalability for producing high-quality and impurity-free few-layer BNNSs from the boron nitride powders.
b. Tribological tests revealed that BNNSs demonstrate excellent friction-reducing and anti-wear properties in GTL. Furthermore, the findings indicate that at a BNNS content of 0.8 wt.%, the system displayed the lowest COF and WSD. Particularly, with an addition of 0.8 wt.% BNNS into GTL, the AFC and WSD were reduced significantly by 40.1% and 35.4%, by comparison with pure base oil, respectively, and the surface roughness, wear depth, and wear volume were effectively reduced by 91.0%, 68.5%, and 76.8%, compared to GTL base oil, respectively.
c. The Raman, SEM-EDS, and XPS results proved that the prominent friction-reducing and anti-wear properties of BNNS could primarily be ascribed to the presence of the physical adsorption film and tribo-chemical film, which were composed of FeOOH, FeO, Fe_3O_4, and B_2O_3.

Author Contributions: Investigation, J.L., S.X., X.Z., S.L. and K.D.; resources, S.X., S.L. and Y.L. (Yuehao Liu); methodology and validation, S.X., X.Y. and Q.Z.; visualization and formal analysis, J.L., D.H. and K.X.; supervision, J.L., S.L., B.X. and K.M.; writing—original draft preparation, S.X., S.L., G.L. and Y.L. (Yiwei Liu); writing—review and editing, J.L., S.X., S.L., Y.F., G.L., Y.L. (Yiwei Liu), D.H. and K.D. All authors have read and agreed to the published version of the manuscript.

Funding: This research was funded by Science and Technology Research Program of Chongqing Municipal Education Commission, grant number KJZD-K202212905, and Natural Science Foundation of Chongqing, grant number cstc2019jcyj-msxmX0453.

Data Availability Statement: The original contributions presented in the study are included in the article. Further inquiries can be directed to the corresponding author.

Conflicts of Interest: Authors Yunhong Fan, Yuehao Liu, Bingxue Xiong and Kai Ma were employed by the Sinopec Lubricant Co., Ltd. The remaining authors declare that the research was conducted in the absence of any commercial or financial relationships that could be construed as a potential conflict of interest.

References

1. Liang, Z.; Wang, S.; Zhu, K.; Chen, Y.; Wei, F.; Chen, D. Enhancing the tribological properties and corrosion resistance of graphene-based lubricating grease via ultrasonic-assisted ball milling. *Colloids Surf. A Physicochem. Eng. Asp.* **2022**, *633 Pt 2*, 127889. [CrossRef]
2. Cheng, Z.; Qin, X. Study on friction performance of graphene-based semi-solid grease. *Chin. Chem. Lett.* **2014**, *25*, 1305–1307. [CrossRef]

3. Krylov, S.Y.; Frenken, J.W.M. Atomistic mechanisms for frictional energy dissipation during continuous sliding. *Sci. Rep.* **2021**, *11*, 19964. [CrossRef]
4. Guan, J.; Xu, Z.; Zheng, L.; Yang, L.; Huang, S. Self-lubricating properties of polyether-ether-ketone composites filled with CNTs@RC2540 nano-capsules. *Lubricants* **2023**, *11*, 511. [CrossRef]
5. Liu, X.; Wang, L.; Xue, Q. DLC-based solid–liquid synergetic lubricating coatings for improving tribological behavior of boundary lubricated surfaces under high vacuum condition. *Wear* **2011**, *271*, 889–898. [CrossRef]
6. Zhang, X.; Xue, S.; Yan, Y.; Liu, S.; Ye, Q.; Zhou, F. Mechanochemical Synthesis of Thiadiazole Functionalized COF as Oil-Based Lubricant Additive for Reducing Friction and Wear. *Langmuir* **2024**, *40*, 4373–4381. [CrossRef] [PubMed]
7. Jiang, Z.; Wu, J.; Yu, L.; Bi, J.; Wang, Y.; Hu, X.; Zhang, Y.; Li, W. Two-dimensional nanomaterials as lubricant additives: The state-of-the-art and future prospects. *J. Mater. Chem. C* **2025**, *13*, 4327–4373. [CrossRef]
8. Yang, C.; Wang, G.; Guo, S.; Sun, J. Potential and progress of two-dimensional nanomaterials in oil-based lubrication. *Chin. Chem. Lett.* **2025**, 111178. [CrossRef]
9. Scherge, M.; Böttcher, R.; Kürten, D.; Linsler, D. Multi-Phase Friction and Wear Reduction by Copper Nanoparticles. *Lubricants* **2016**, *4*, 36. [CrossRef]
10. He, X.; Stevenson, L.M.; Kumara, C.; Mathews, T.J.; Luo, H.; Qu, J. Comparison of eco-friendly ionic liquids and commercial bio-derived lubricant additives in terms of tribological performance and aquatic toxicity. *Molecules* **2024**, *29*, 3851. [CrossRef]
11. Ankit, K.; Pranami, R.; Satyanarayana, G.R. Thermophysical and tribological properties of nanolubricants: A review. *Heat Mass Transf.* **2018**, *54*, 3493–3508.
12. Alireza, F.; Vahab, G.; Fatemeh, A. The experimental comparison between the effect of copper oxide and graphene nanoparticles on rheological behavior and thermal properties of engine oil. *Pet. Sci. Technol.* **2022**, *40*, 803–821.
13. Wang, Q.; Wang, L.; Zhao, S.; Meng, Z. Experimental study on the suspension stability and tribological properties of nano-copper in LCKD-320# lubricating oil. *Appl. Nanosci.* **2020**, *11*, 45–54.
14. Xu, J.; Lu, H.; Lian, J. The influence of the particle size and size synergistic effect of nano-copper on the tribological properties of lubricants. *Tribol. Int.* **2025**, *201*, 110282. [CrossRef]
15. Han, Y.; Pan, L.; Zhang, H.; Zeng, Y.; Yin, Z. Effect of lubricant additives of Cu, Fe and bimetallic CuFe nanoparticles on tribological properties. *Wear* **2022**, *508*, 204485. [CrossRef]
16. Li, J.; Chen, D.; Zhang, H.; Jiang, Z.; Sun, K.; Fan, J.; Tang, Y. The tribological properties of nano-lubricants and their application on bearings: Recent research progress. *Int. J. Adv. Manuf. Technol.* **2024**, *134*, 3051–3082. [CrossRef]
17. Li, T.; He, Y.; Zhang, C.; Xue, H.; Zhong, Y.; Gu, L.; Wu, L. Remarkable lubricity of CNTs microspheres as additives in oil lubricant for ceramic components. *Ceram. Int.* **2024**, *50*, 1411–1418. [CrossRef]
18. Wang, W.; Zhang, G.; Xie, G. Ultralow concentration of graphene oxide nanosheets as oil-based lubricant additives. *Appl. Surf. Sci.* **2019**, *498*, 143683. [CrossRef]
19. Shen, M.; Li, B.; Zhang, Z.; Zhao, L.; Xiong, G. Abrasive wear behavior of PTFE for seal applications under abrasive-atmosphere sliding condition. *Friction* **2019**, *8*, 755–767. [CrossRef]
20. Martins, A.S.; Valdicleide, S.E.M.; Amilton, S. Nanolubrication Mechanisms: Influence of Size and Concentration of CuO Nanoparticles. *Mater. Perform. Charact.* **2018**, *7*, 226–241.
21. Sun, W.; Zhou, Z.; Liu, J. The size effect of SiO_2 particles on friction mechanisms of a composite friction material. *Tribol. Lett.* **2018**, *66*, 35. [CrossRef]
22. Dong, S.; Wang, W.; Gao, Y.; Deng, G. Tribological properties of different-sized black phosphorus nanosheets as water-based lubrication additives for steel/titanium alloy wear contact. *Metals* **2022**, *12*, 288. [CrossRef]
23. Shan, Z.; Jia, X.; Tian, R.; Yang, J.; Su, Y.; Song, H. In-situ exfoliation of large sized h-BNNS by esterified nanocellulose to build aqueous lubricants that can switch between liquid and gel states. *Tribol. Int.* **2023**, *188*, 108843. [CrossRef]
24. Kumari, S.; Chouhan, A.; Sharma, O.P.; Tawfik, S.A.; Spencer, M.J.S.; Bhargava, S.K.; Walia, S.; Ray, A.; Khatri, O.P. Alkali-Assisted Hydrothermal Exfoliation and Surfactant-Driven Functionalization of h-BN Nanosheets for Lubrication Enhancement. *ACS Appl. Nano Mater.* **2021**, *4*, 9143–9154. [CrossRef]
25. Yang, W.; Geng, Z.; Li, Y.; Liu, X.; Tian, X.; Wang, S.; Wu, N.; Wang, Y.; Xu, R.; Yang, F.; et al. Facile synthesis of lipophilic alkylated boron nitride nanosheets as lubricating oil additive to greatly enhance the friction and heat-conducting properties. *Tribol. Int.* **2022**, *173*, 107655. [CrossRef]
26. Kumar, N.; Saini, V.; Bijwe, J. Tribological investigations of nano and micro-sized graphite particles as an additive in lithium-based grease. *Tribol. Lett.* **2020**, *68*, 124. [CrossRef]
27. Zhang, B.; Wu, Q.; Yu, H.; Bulin, C.; Sun, H.; Li, R.; Ge, X.; Xing, R. High-efficient liquid exfoliation of boron nitride nanosheets using aqueous solution of alkanolamine. *Nanoscale Res. Lett.* **2017**, *12*, 596. [CrossRef]
28. Qin, Y.; Wu, M.; Yang, G.; Yang, Y.; Zhao, L. Tribological performance of magnesium silicate hydroxide/Ni composite as an oil-based additive for steel–steel contact. *Tribol. Lett.* **2021**, *69*, 19. [CrossRef]

29. Yuan, F.; Jiao, W.; Yang, F.; Liu, W.; Liu, J.; Xu, Z.; Wang, R. Scalable exfoliation for large-size boron nitride nanosheets by low temperature thermal expansion-assisted ultrasonic exfoliation. *J. Mater. Chem. C* **2017**, *5*, 6359–6368. [CrossRef]
30. Shan, Q.; Shi, X.; Wang, X.; Wu, W. Preparation of functionalized boron nitride nanosheets by high-gravity liquid phase exfoliation technology. *Chem. Eng. Process.-Process Intensif.* **2021**, *169*, 108602. [CrossRef]
31. Zhu, J.; Lu, Z.; Aruna, S.T.; Doron, A.; Aharon, G. Sonochemical synthesis of SnO_2 nanoparticles and their preliminary study as Li insertion electrodes. *Chem. Mater.* **2000**, *12*, 2557–2566. [CrossRef]
32. Shang, J.; Xue, F.; Fan, C.; Ding, E. Preparation of few layers hexagonal boron nitride nanosheets via high-pressure homogenization. *Mater. Lett.* **2016**, *181*, 144–147. [CrossRef]
33. Lin, K.; Zhuang, Z.; Li, Y.; Zeng, Z.; Wei, X.; Fan, X.; Zhu, M. Well-dispersed graphene enhanced lithium complex grease toward high-efficient lubrication. *Chin. J. Mech. Eng.* **2023**, *36*, 133. [CrossRef]
34. Jiang, H.; Hou, X.; Qian, Y.; Liu, H.; Kamal, A.A.M.; Dearn, K.D. A tribological behavior assessment of steel contacting interface lubricated by engine oil introducing layered structural nanomaterials functionalized by oleic acid. *Wear* **2023**, *524*, 204675. [CrossRef]
35. Du, C.; Yu, T.; Wu, Z.; Zhang, L.; Shen, R.; Li, X.; Feng, M.; Feng, Y.; Wang, D. Achieving macroscale superlubricity with ultra-short running-in period by using polyethylene glycol-tannic acid complex green lubricant. *Friction* **2023**, *11*, 748–762. [CrossRef]
36. Chen, H.; Xiao, G.; Chen, Z.; Yi, M.; Zhang, J.; Li, Z.; Xu, C. Hexagonal boron nitride (h-BN) nanosheets as lubricant additive to 5CB liquid crystal for friction and wear reduction. *Mater. Lett.* **2022**, *307*, 131007. [CrossRef]
37. Liu, L.; Jiao, S.; Peng, Y.; Zhou, W. A Green Design for Lubrication: Multifunctional System Containing Fe_3O_4@MoS_2 Nanohybrid. *ACS Sustain. Chem. Eng.* **2018**, *6*, 7372–7379. [CrossRef]
38. Lei, X.; Zhang, Y.; Zhang, S.; Yang, G.; Zhang, C.; Zhang, P. Study on the mechanism of rapid formation of ultra-thick tribofilm by CeO_2 nano additive and ZDDP. *Friction* **2022**, *11*, 48–63. [CrossRef]
39. Zhao, Y.; Luo, C.; Zhang, J.; Zhang, X.; Wang, F.; Bai, C. A strategy of hexagonal boron nitride endowing lubricant oil with steady superlubricity. *Appl. Surf. Sci.* **2025**, *697*, 163060. [CrossRef]

Disclaimer/Publisher's Note: The statements, opinions and data contained in all publications are solely those of the individual author(s) and contributor(s) and not of MDPI and/or the editor(s). MDPI and/or the editor(s) disclaim responsibility for any injury to people or property resulting from any ideas, methods, instructions or products referred to in the content.